Retrieval of ozone profiles from OMPS limb scattering observations

Carlo Arosio[1], Alexei Rozanov[1], Elizaveta Malinina[1], Kai-Uwe Eichmann[1], Thomas von Clarmann[2], and John P. Burrows[1]

[1]Insitute of Environmental Physics, University of Bremen, Bremen, Germany
[2]Karlsruhe Institute of Technology, Karlsruhe, Germany

Correspondence to: carloarosio@iup.physik.uni-bremen.de

Abstract. This study describes a retrieval algorithm developed at the University of Bremen to retrieve vertical profiles of ozone from limb observations performed by the Ozone Mapper and Profiler Suite (OMPS). This algorithm was originally developed for use with data from the SCanning Imaging Absorption spectroMeter for Atmospheric CHartographY (SCIAMACHY) instrument. As both instruments make limb measurements of the scattered solar radiation in the Ultraviolet (UV) and Visible (Vis) spectral ranges, an underlying objective of the study is to obtain consolidated and consistent ozone profiles from the two satellites and to produce a combined data set. The retrieval algorithm uses altitude-normalized radiances in the UV and Vis wavelength ranges to obtain ozone concentrations in 12–60 km altitude range. Measurements at altitudes contaminated by clouds in the instrument field of view are identified and filtered. An independent aerosol retrieval is performed beforehand and its results are used to account for the stratospheric aerosol load in the ozone retrieval. The typical vertical resolution of the retrieved profiles varies from $\sim$ 2.5 km at lower altitudes (< 30 km) to $\sim$ 1.5 km at upper altitudes (from 40 km to just below top levels). The retrieval errors resulting from the measurement noise are estimated to be 1–5 % above 25 km, increasing to 10–15 % below 20 km. OMPS ozone profiles are retrieved for seven months, from July 2016 to January 2017. Results are compared with NASA ozone profile product and validated against profiles derived from passive satellite observations, or measured by balloon-borne in situ sondes. Between 20 and 50 km, OMPS ozone profiles typically agree with data from the Microwave Limb Sounder (MLS) v4.2 within 5–10 %, with the exception of high northern latitudes (> 70° N above 40 km) and the tropical lower stratosphere. The comparison of OMPS profiles with ozonesonde measurements shows differences within $\pm$5 % between 14 and 30 km at northern mid-latitudes. At southern mid-latitudes, an agreement within 5–10 % is achieved, although these results are less reliable because of a limited number of available coincidences. An unexpected bias of approximately 10 % is detected in the tropical region at all altitudes. The processing of the 2013 data set using the same retrieval settings and its validation against ozonesondes reveals a much smaller bias; possible reasons for this behavior are under investigation.

1 Introduction

Ozone is one of the most important trace gases in the atmosphere. It is most abundant in the stratospheric 'ozone layer', which absorbs strong ultraviolet (UV) radiation, heating this atmospheric region and acting as a protective layer against biologically harmful radiation. It plays a crucial role in the radiative budget of the stratosphere, determines the tropopause height and thus also impacts on climate. After the recognition that man-made release of chlorofluorocarbon compounds depletes the strato-

spheric ozone layer (Molina and Rowland, 1974) and the discovery of the springtime ozone hole in Antarctica (Farman et al., 1985), research grew in this field because of its relevance to both science and society. Although nowadays the stratospheric ozone chemistry is generally well understood, there are still several issues to be clarified. These are related to the expected ozone recovery after the adoption of the Montreal protocol, stratospheric responses to changes in tropospheric radiative fluxes and temperatures as well as long term ozone trends. For example, Solomon et al. (2016) focused the attention on the Antarctic region, investigating possible signatures of an ozone healing. Analyzing observations collected each September since 2000, the authors suggested that the fingerprints of an ozone recovery can be identified in both the increase of its column amount and in the decrease of the areal extent of the ozone hole.

The issues related to changes in the Brewer Dobson Circulation (BDC), possibly linked to climate changes, have been investigated by several studies, which consider the ozone concentration in the lower stratosphere a good proxy to track changes in the stratospheric circulation. Among them, Aschmann et al. (2014) used combined O_3 time series from satellite instruments and ozonesondes to investigate changes in the BDC after the beginning of the century and identified an asymmetry in the BDC northern and southern branches. Stiller et al. (2017) suggested a shift of the subtropical mixing barriers as an explanation for this asymmetry.

For all these kinds of studies, reliable long-term data sets are needed from both ground-based and satellite instruments. Recent attempts to consistently merge a large number of different data sets into long-term time series are reported by Froidevaux et al. (2015) and Davis et al. (2016) both including also other species than ozone. Steinbrecht et al. (2017) and Sofieva et al. (2017) focused on ozone trends, revealing a global statistically significant increase in its amount after 2000 above 35 km. Other authors, as Kyrölä et al. (2013), Eckert et al. (2014), Gebhardt et al. (2014) and Nedoluha et al. (2015) pointed out an unexpected decadal negative trend in the ozone abundance in the upper tropical stratosphere.

During the last few decades, several remote sensing observation techniques have been used to derive ozone concentrations from the troposphere up to the mesosphere (Hassler et al., 2014). Following the birth of the space age, instrumentation of different kinds began to be developed. Space-borne remote sensing measurements in the Ultraviolet-Visible (UV-Vis) spectral range have traditionally been of two types: nadir viewing and solar occultation spectrometers; the former instruments point downward and are characterized by a good horizontal coverage whereas the latter look directly into the solar disk, featuring a good vertical resolution and a strong signal. The limb sounding technique, widely used by more recent satellite instruments, combines the advantage of these two: the long path through the atmosphere provides a high sensitivity to trace gases and the variation of the observation angle enables a better vertical resolution with respect to the nadir geometry, featuring a much higher horizontal sampling as compared to the occultation measurements. Limb observation geometry has also been used to measure scattered solar radiance and/or atmospheric emission in the InfraRed (IR) and microwave spectral regions. Using the scattered solar light, measurements during daylight only are possible, whereas, using the emission signatures, observations can be performed during both day and night. With decreasing altitude the atmosphere becomes more opaque, which results in a decreasing sensitivity of the limb-scatter measurements in the troposphere.

The limb scatter technique was for the first time successfully exploited by the LORE/SOLSE (Limb Ozone Retrieval Experiment/Shuttle Ozone Limb Sounding Experiment) instrument launched in 1997 by NASA. Two instruments followed this mis-

sion: the Optical Spectrograph and Infrared Imager System (OSIRIS) launched in February 2001 (Llewellyn et al., 1997) and the SCanning Imaging Absorption spectroMeter for Atmospheric CHartographY (SCIAMACHY), launched in March 2002 (Burrows et al., 1995; Gottwald and Bovensmann, 2011). SCIAMACHY made observations in the UV, Vis, Near InfraRed (NIR) and Short Wave InfraRed (SWIR) spectral ranges till April 2012, when the platform-to-ground communication was lost. A few aging satellite instruments, such as OSIRIS and the Microwave Limb Sounder (MLS), are still operating, contributing to the task of continuous monitoring the stratospheric ozone. At the end of 2011, just a few months before the end of ENVISAT lifetime, the Ozone Mapping and Profiler Suite (OMPS) instrument was launched on board the Suomi-National Polar-Orbiting Operational Environmental Satellite System Preparatory Project (SNPP) platform and it is still operational (Flynn et al., 2014). The spacecraft has a nominal 13:30 local time ascending sun-synchronous orbit and flies at a mean altitude of 833 km. Scientific data collection started at the beginning of 2012. OMPS comprises three instruments: the Nadir Mapper, Nadir Profiler and Limb Profiler (LP). Only the latter is of interest for our study (see Flynn et al., 2014, for a review of the full suite).

After the launch of the satellite, the NASA team developed a retrieval chain to derive ozone profiles and many by-products from OMPS limb observations, which are publicly available. Besides, at the University of Saskatchewan a 2-D geometry retrieval has been applied to OMPS-LP measurements (Zawada et al., 2017).

This paper presents ozone profile retrievals from OMPS-LP observations performed at the University of Bremen. The algorithm we use was adapted from the SCIAMACHY v3.0 ozone retrieval (Jia et al., 2015). The underlying objective of the study is the creation of a consolidated data set and the merging of the OMPS and the SCIAMACHY time series, in order to obtain a long-term continuous data set. In Sect. 2, the OMPS instrument is introduced: its geometry of observation, relevant characteristics and issues related to the retrieval of ozone are briefly discussed. The third section is focused on the retrieval methodology, starting with a general description of the inversion algorithm used in this work. A more detailed characterization of the retrieval procedure follows, including the applied cloud filter and the approach to consider aerosol extinction profiles. Sect. 4 presents at first a comparison with NASA ozone profile retrieval algorithm; then MLS and ozonesonde data sets are used for a first validation of our results. Main results, remaining issues and possible future improvements are addressed in the conclusions.

2 OMPS-LP instrument

2.1 General features

The main objective of OMPS-LP is to monitor the ozone vertical distribution within the Earth middle atmosphere at high accuracy level. It images the Earth atmosphere by viewing its edge (limb) from space. The closest approach of the sensor line of sight to the Earth surface is referred to as Tangent Point (TP) and the altitude of this point above the Earth geoid is called Tangent Height (TH); the limb geometry is schematically drawn in Fig. 1.

The OMPS-LP sensor views at the Earth limb backwards with respect to the flying direction, through three vertical slits: the central one is aligned along the nadir track, whereas the other two are cross-track, separated horizontally by 4.25°, which corresponds to 250 km distance between the TPs. With respect to the satellite, the TPs are located on the East, around 25°

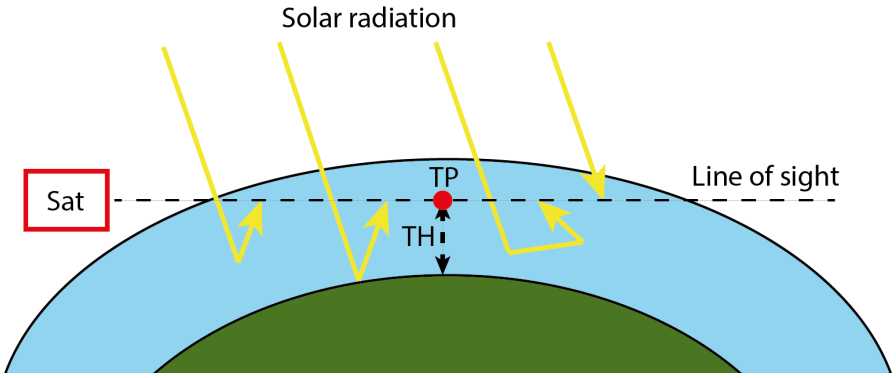

Figure 1. Schematic diagram of the viewing geometry of a satellite limb observation, showing the so called Tangent Point (TP) and its height above the Earth, or Tangent Height (TH).

latitude South of the sub-satellite point. The geometry is drawn in Fig. 2. The spacecraft completes 14–15 orbits per day and the instrument performs normally 180 limb observations (referred to as states) per orbit, around 160 of which with solar zenith angle less then 80°.

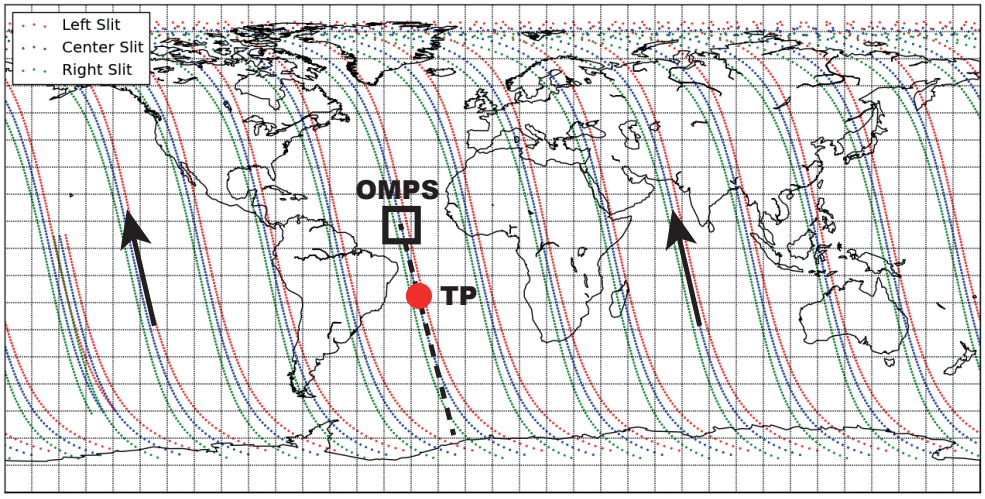

Figure 2. OMPS daily orbits and observation geometry sketch; black arrows indicate the satellite flight direction and the red dot approximately locates the Tangent Point (TP). Adapted from Bhartia et al. (2013).

OMPS-LP measures limb scattered radiance in the spectral range of 280–1000 nm. A particular characteristic of this instrument is the use of a prism spectrometer instead of a grating disperser. The employed prism provides a spectral resolution that degrades with the wavelength, from 1 nm in the UV region up to 40 nm in the NIR. OMPS-LP observes the full altitude range at the same time, without vertical scanning: each slit covers a vertical range of 112 km, with an instantaneous field of view of

about 1.5 km and a sampling of 1 km at TP (Jaross et al., 2014). Radiance is collected by means of a Charge-Coupled Device (CCD). The use of such a technology poses a great challenge as regards the dynamic range: indeed, due to the decrease of the atmospheric density, scattered solar radiance from the Earth limb decreases by at least five orders of magnitude along the considered vertical range. Therefore, in order to cover the required dynamic range, four images at a 2-D physical CCD are taken for each slit: the full atmosphere is imaged at two integration times (that differ by a factor 30) and through a large and a small aperture (Jaross et al., 2014). Since the down-link rate is by far slower than the data collection rate, only a selected number of pixels from these four images can be transferred. Then, ground processing is needed to select unsaturated signals and combine down-linked pixels from different images in a single radiance file. The combined image features a non-uniform wavelength and TH grid (spectral and vertical smile), therefore it is re-sampled and mapped onto a regular grid. Fig. 3 shows examples of radiance profile, displaying the large dynamic range of measured values. The gridding procedure is performed using a bi-linear interpolation and pixel-to-pixel calibration errors linked to this consolidation procedure are estimated to be around 1 %. As radiance measured at large and small aperture can differ by several percent, radiance profiles at a specific wavelength are derived from one aperture only; on the contrary, a better consistency is found between long and short integration time, so that they are combined at different altitudes to get each radiance profile. Fig. 4 shows examples of spectral signal-to-noise ratio at different altitudes. Jumps in this plot are related to changes of the sampled image: for example, the jump between large and small aperture that occur at 450 nm (fixed threshold). In the retrieval scheme we were careful not to consider spectral ranges crossing this fixed boundary.

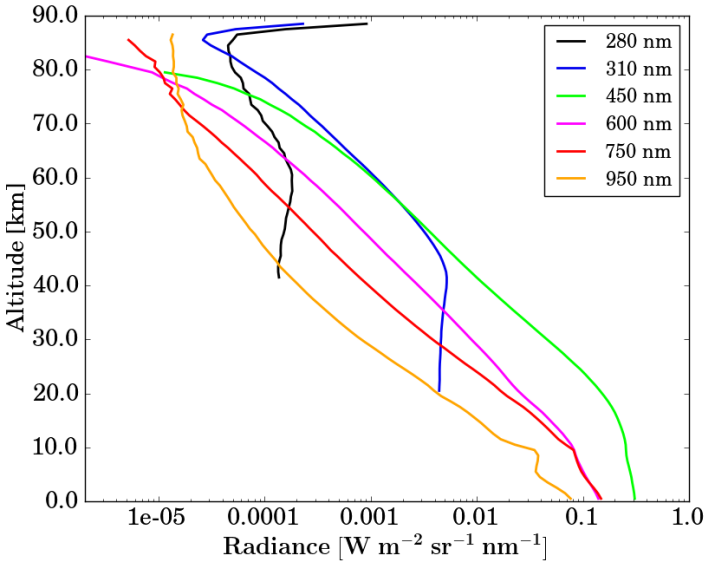

Figure 3. Example of OMPS-LP radiance profiles at some selected wavelengths.

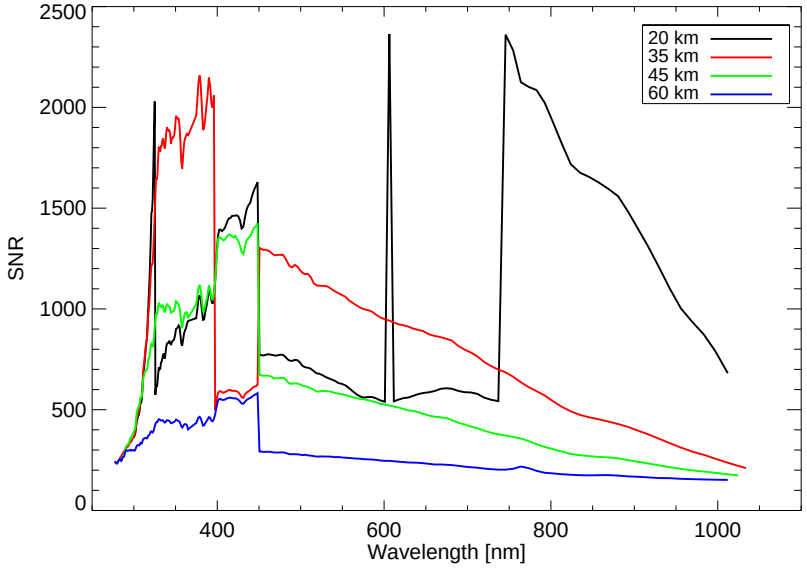

Figure 4. Example of OMPS-LP signal-to-noise ratio at different tangent heights.

2.2 Calibration and main issues

One of the most important issues that affects the quality of the limb scattering technique is the TH registration. In order to retrieve reliable ozone profiles, the TP altitude has to be known with high precision: in fact, a 200 m uncertainty in the TP height translates into a 5 % error in the ozone profile. Such a high accuracy cannot be directly reached for OMPS-LP sensor, because the star-tracker on board the SNPP satellite is mounted on a distant position from the instrument, so that thermal effects and mis-alignments of the instrument focal plane play an important role.

To solve this problem, two methods called Rayleigh Scattering Altitude Sensing (RSAS) and Absolute Radiance Residual method (ARRM) are implemented by the NASA team in the level 1b gridded (L1G) data processing (Moy et al., 2017). Fixed adjustments between 1 and 2 km are applied independently for each slit, meaning that the instrument points at altitudes higher than expected. A TH variation related to the heating up of the instrument is detected when the instrument approaches northern mid-latitudes. It is accounted for in L1G data applying a latitudinal dependent correction on the order of 500 m for every orbit. This correction remains the same for every orbit. A further dynamic TH variation was detected within each orbit, with an almost linear dependence with latitude. The current estimate is around 400 m change between the South and the North Pole. A satisfactory explanation for this variation still has to be found and this effect is not currently corrected neither in L1G data nor in our retrievals.

The second important issue that affects the accuracy of the limb radiance is the so-called stray light. The general phenomenon of stray light describes photons that are registered by the detector at wavelengths or altitudes which they do not belong to. There are several causes of the stray light. For example, with multiple images on a single detector, photons from the IR part of one slit can be scattered into the UV part of the neighboring image. This problem was reduced with both a thorough study of the

point spread function during the pre-launch operations and the careful application of cutoff filters at the focal plane (Jaross et al., 2014). Stray light is mainly an issue at high altitudes, with levels that are usually less than 10 % of the measured value and tend to increase with the altitude for the same wavelength.

The CCD used for detection of photons for OMPS-LP operates at -45 °C to minimize dark current and other noise sources. Dark current and non-linearity of the sensor are corrected accurately and introduce minor errors in the reported radiance. Transient events can affect the instrument reliability: energetic charged particle can penetrate through the CCD shielding and cause transients in pixel signal. Such events are frequent in the so-called South Atlantic anomaly.

In this paper, version 2.5 of OMPS-LP L1G data has been used without any additional pre-processing related to stray light and pointing. The treatment of stray light has been improved with respect to the previous version and pointing corrections implemented as discussed above. In addition, both sun-normalized and absolute radiances are provided.

2.3 OMPS-LP observation geometry

Several angular coordinates are needed in the retrieval algorithm to correctly describe the observation geometry; satellite azimuth (φ), solar azimuth (φ_0) and solar zenith angle (ψ_0) at the TP are reported for three THs (25, 35 and 45 km) in the L1G data files and are used to define the geometry of the observation. The solar zenith angle (ψ_0) is defined as the angle between the local vertical at the TP and the sun pointing vector. The azimuth angles (φ and φ_0) are defined as the angles between the direction to North Pole and the projections of the solar beam and the instrument line of sight, respectively, on the plane orthogonal to the normal vector at the TP.

Combining azimuth and zenith angles, the scattering angle θ at the TP can be computed as:

$$\cos(\theta) = \sin(\psi_0)\cos(\varphi - \varphi_0) \tag{1}$$

This is an important quantity that defines the scattering geometry. In Fig. 5 values of scattering angles together with solar zenith angles are plotted as a function of latitude for three OMPS orbits in different seasons. Solar zenith angles are shown as solid lines, with symmetric values with respect to the equatorial region, whereas scattering angles are plotted as dashed lines. Only solar zenith angles less than 80° are plotted and the ozone retrieval is run only for the corresponding states to avoid high stray light levels. The latitude coverage in different seasons can be assessed from the figure.

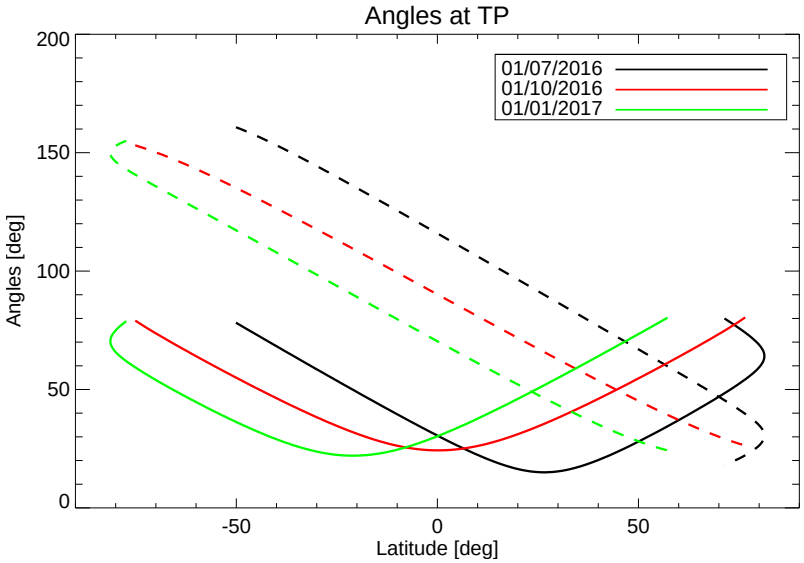

Figure 5. Solar zenith angles (solid lines) and scattering angles (dashed lines) at the TP along three OMPS orbits on the following dates: Jul 1, 2016, Oct 1, 2016 and Jan 1, 2017.

3 Retrieval method

3.1 Theoretical basis

The retrieval of ozone profiles is performed using the regularized inversion technique with the first order Tikhonov constraints (Tikhonov, 1963; Rodgers, 2000). The non-linearity of the inverse problem is accounted for using an iterative approach. The forward modeling takes into consideration atmospheric multiple scattering in the framework of the approximate spherical solver of the SCIATRAN radiative transfer model (Rozanov et al., 2014). Thereby, the CDI (Combined Differential-Integral) approach is employed to solve the radiative transfer equation: first, the entire radiation field is calculated in the pseudo-spherical approximation for a set of solar zenith angles using the finite difference method. Pseudo-spherical approximation means that the single scattering contribution is calculated in a fully spherical geometry while a plane parallel atmosphere is assumed to calculate the multiple scattering contribution (Rozanov et al., 2000). Then, an integration along the line-of-sight is carried out in a spherical geometry, i.e. intersecting a spherical shell atmosphere, accounting also for the atmospheric refraction. Thereby, the pseudo-spherical radiative field calculated at the first step is used to approximate the multiple scattering contribution at each point along the line of sight. The weighting functions are calculated using the same method as for the radiance, but considering only the single scattering contribution.

Linearizing the forward model around an initial guess state $\boldsymbol{x_0}$, the general equation that has to be solved can be written as:

$$\boldsymbol{y} = \boldsymbol{y_0} + \mathbf{K}(\boldsymbol{x} - \boldsymbol{x_0}) + \boldsymbol{\epsilon} \tag{2}$$

where $\boldsymbol{y}$ is the measurement vector, $\boldsymbol{y_0}$ is the simulated spectrum, $\mathbf{K}$ is the linearized forward model operator represented by the weighting function matrix, $\boldsymbol{x}$ is the state vector and ϵ represents errors of any kind. Following (Rodgers, 2000), the solution of Eq. (2) can be estimated iteratively. Taking into consideration that in our algorithm the retrieval is performed from a zero a priori profile, the iterative step $i+1$ can be expressed as:

$$\boldsymbol{x_{i+1}} = (\mathbf{K_i^T S_\epsilon}^{-1}\mathbf{K_i} + \mathbf{S_0} + \mathbf{S_1^T}\boldsymbol{\gamma}\mathbf{S_1})^{-1}\mathbf{K_i^T S_\epsilon}^{-1}(\boldsymbol{y} - \boldsymbol{y_i} + \mathbf{K_i}\boldsymbol{x_i}) \tag{3}$$

Here, $\mathbf{S}_\epsilon$ is the measurement noise covariance matrix. $\mathbf{S_0}$ is the diagonal matrix optimized to constrain the solution within physically meaningful values and minimize a possible negative bias caused by the use of a zero a priori profile. The effect of the chosen matrix is significant only at tropical low altitudes and globally at high altitudes, where the ozone concentration is very small. Finally, $\mathbf{S_1}$ is the first order derivative matrix ($\mathbf{S_1^T}\boldsymbol{\gamma}\mathbf{S_1}$ is the first order Tikhonov term). It is multiplied by the diagonal matrix $\boldsymbol{\gamma}$ which contains altitude dependent weights, used to constrain the smoothness of the retrieved profile. In the following, the sum $\mathbf{S_0} + \mathbf{S_1^T}\boldsymbol{\gamma}\mathbf{S_1}$ will be named as $\mathbf{S_r}$.

3.2 Algorithm implementation

For the ozone vertical profile retrieval from OMPS-LP, four spectral segments are selected: three in the UV spectral region (Hartley and Huggins bands) and one in the visible range (Chappuis band); the former ranges are sensitive to the upper stratospheric ozone, whereas the latter to the lower stratospheric region, where the peak of the number density occurs. In order to avoid strong absorption bands of water vapor and O_2, wavelengths in the ranges 580.0–607.0 nm and 620.0–635.0 nm are rejected. A complete treatment of these absorption features requires line-by-line calculations, that are computationally expensive. The altitude range over which the retrieval is performed spans between 12 and 60 km above the sea level. The vertical grid is fixed throughout the processing and covers the retrieval range at evenly spaced steps of 1 km. To prepare the measurement vector, limb radiance in each spectral interval is normalized with respect to a limb measurement at an upper TH, in order to provide a self calibration of the instrument and reduce the effect of surface/cloud reflectance. In addition, for longer wavelength intervals, a polynomial is subtracted from the logarithm of the normalized radiance in order to remove slowly-variable spectral features, e.g. caused by aerosol scattering (Rozanov et al., 2011). Eq. (4) explicitly shows the measurement vector at the i-th TH and details about spectral segments and TH normalizations are listed in Table 1. The last column provides the information about the subtracted polynomial in the measurement vector: first order in the visible range, zeroth order or no polynomial in the UV region.

$$\boldsymbol{y_i} = \log\left(\frac{\boldsymbol{I_{TH_i}}}{\boldsymbol{I_{TH_{norm}}}}\right) - \boldsymbol{P_n} \tag{4}$$

In the forward model, the radiation is calculated taking into account O_3, NO_2 and O_4, which have spectral signatures in the selected spectral ranges. Cross sections of these gases are taken from Serdyuchenko et al. (2014), Bogumil et al. (2000) and Hermans (2011), respectively. Cross sections are beforehand convolved to the OMPS-LP spectral resolution. Ancillary pressure and temperature profiles are taken from the Global Modeling and Assimilation Office (GMAO) interpolated data set, provided by the NASA team together with OMPS-LP L1G radiances.

Table 1. List of the spectral segments considered for the ozone retrieval with corresponding altitude ranges, THs used for the normalization and order of the subtracted polynomial (- means that no polynomial is subtracted).

Altitude range [km]	Spectral segment [nm]	Normalization TH [km]	Polynomial order
46-60	285-300	63	-
35-46	305-313	52	-
31-36	322-331	47	0
12-33	508-660 †	42	1

† 580.0–607.0 and 620.0–635.0 nm ranges are rejected.

Before the main retrieval procedure, a shift and squeeze correction is applied in the Chappuis band to the modeled spectrum with respect to the measured one. This pre-processing is performed for each observation at each TH independently and is introduced to account for issues related to the spectral calibration and possible thermal expansion of the detector. Typical values for the spectral shift are inside the range [+1,+4] nm for the first point of the interval and [-2,+1] nm for the last spectral point. As the shift and squeeze correction algorithm works with the differential absorption structures, it cannot be applied in the UV range. Furthermore, as the UV retrieval uses either normalized radiances themselves or their slopes, the influence of a possible spectral misalignment is rather small. In the pre-processing procedure, we obtain the $\mathbf{S}_\epsilon$ matrix from the fit residuals, fitting absorption features of all relevant gases in the selected spectral windows.

The inversion scheme is then iteratively run employing the Eq. (3). The state vector $\boldsymbol{x_{i+1}}$, containing the retrieved ozone vertical distribution at each iteration, is expressed in terms of the Volume Mixing Ratio (VMR), which is more suitable for use with smoothing constraints. The smoothing weights, i.e. square roots of the diagonal elements of $\boldsymbol{\gamma}$, linearly increase with the height above 45 km and remain constant below.

Surface albedo is simultaneously retrieved with ozone using the sun-normalized radiance provided in the L1G data. Two spectral fitting windows at THs around 38 km are employed: 355–365 nm and 455–470 nm, where ozone absorption is weak.

3.3 Cloud filter

A cloud filter is applied during the ozone retrieval to reject THs at which a cloud is present in the field of view of the instrument. The applied algorithm is based on the Color Index Ratio (CIR) concept (Eichmann et al., 2016), using OMPS-LP radiance at 754 nm and 997 nm. The so-called Color Index (CI) is obtained calculating the ratio of the radiance at the two chosen wavelengths for the same OMPS-LP spectrum. The CI is an altitude dependent quantity and can be used to detect the presence of scattering particles in the field of view, since we know the expected ratio for a cloud-free atmosphere. First, the CI is calculated at all THs, then the CIR is obtained as:

$$CIR(z_{TH}) = \frac{CI(z_{TH})}{CI(z_{TH} + \Delta z_{TH})} \tag{5}$$

where Δz_{TH} is the vertical grid step of 1 km. An example of the results for simulated clouds is reported in Fig. 6: cirrus clouds consisting of hexagonal crystals with an optical depth between 0.01 and 0.15 are taken into consideration. Since the ozone retrieval is run above 12 km, we are generally not interested in liquid water clouds.

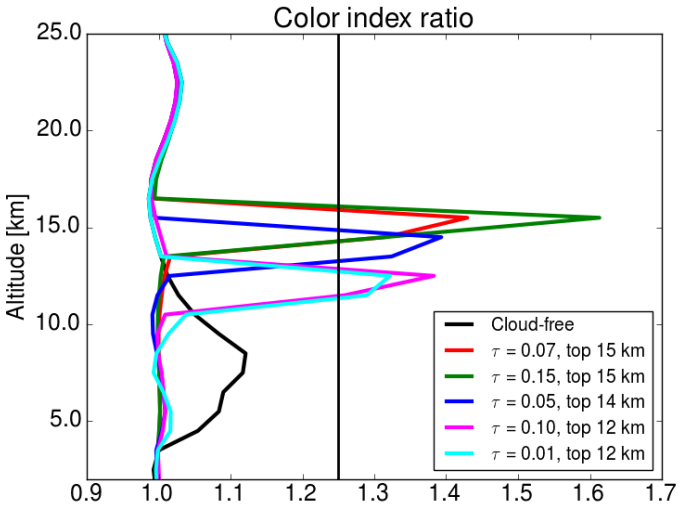

Figure 6. Example of Color Index Ratios for different simulations of ice clouds. Top of the cloud and optical depth (τ) ranges are chosen to simulate the impact of thin cirrus clouds in the upper troposphere.

The chosen threshold to flag a TH as cloudy is 1.25. This technique was also applied to SCIAMACHY measurements with a different threshold (Eichmann et al., 2016). At the considered wavelengths the measured radiation is related to the scattered light from molecules, aerosol or cloud particles. A question may arise regarding the inability of such an approach to distinguish between high aerosol loads and cirrus clouds. Future investigations will focus on a comparison between the CIR filter and aerosol profiles retrieved as described in the next subsection.

A different approach was used to detect Polar Mesospheric Clouds (PMC). The presence of these clouds can affect limb radiance down to 40 km, leading to a bias in the ozone concentration at these altitudes. In clear conditions radiance in the upper stratosphere decreases monotonically with height. To detect the PMC presence, radiance profile around 353 nm is considered for each observation above 50° N and below 50° S: if the radiance between 40 km and 80 km increases for at least two consecutive layers, than the observation is flagged as affected by a PMC. These profiles are rejected throughout all the comparisons with independent data sets.

3.4 Aerosol treatment

The aerosol extinction coefficient is retrieved employing the general approach as used for SCIAMACHY v1.4 stratospheric aerosol extinction product (Rieger et al., 2017). Since OMPS-LP has a coarser spectral resolution than SCIAMACHY, the

retrieval at 750 nm as used for SCIAMACHY is sub-optimal because of the influence of the O_2 absorption band. Instead, a wavelength of 868.8 nm is chosen. Stratospheric aerosol extinction is retrieved in the altitude range from 10.5 km to 33.5 km. The spectrum at 34.5 km is used as the reference; the Lambertian albedo is simultaneously retrieved using the sun-normalized spectrum at 34.5 km. In order to smooth spurious oscillations, the first order Tikhonov regularization is employed. Scattering phase functions are calculated using Mie scattering theory. Thereby, the particle size distribution is assumed to be lognormal with the median radius (r_g) of 0.08 μm, and distribution width parameter (σ) of 1.6. This distribution is described by the following equation:

$$n(r) = \frac{N}{\sqrt{2\pi}\ln(\sigma)r}\exp\left(\frac{(\ln(r_g)-\ln(r))^2}{2\ln^2(\sigma)}\right) \tag{6}$$

The aerosol particles are assumed to be sulfuric droplets with 0 % relative humidity in the surrounding atmosphere. Below 10 km and above 46 km the aerosol load is set to zero. The refractive indexes are calculated using the Optical Properties of Aerosols and Clouds (OPAC) database (Hess et al., 1998). Before using the retrieved aerosol product, altitudes downwards from the detected cloud top height are rejected and each profile is extrapolated by the scaled a priori. The scaling factor is derived averaging three altitude levels above the cloud. The aerosol retrieval is particularly important at latitudes where the scattering angle is high (Fig. 5).

4 Results

OMPS ozone profiles are retrieved for seven months, from July 2006 to January 2007, limited by the availability of v2.5 L1G data at the time of writing this paper. Retrievals were performed using data from the central slit of the instrument only because the lateral slits can still suffer from pointing issues.

4.1 Retrieval characterization and error analysis

The information content of the measurements as well as the sensitivity of the retrieval can be analyzed using the averaging kernels ($\mathbf{A}$) and the covariance of retrieval noise ($\mathbf{S_m}$) obtained respectively as (Rodgers, 2000):

$$\mathbf{A} = (\mathbf{K^T S_\epsilon}^{-1}\mathbf{K} + \mathbf{S_r})^{-1}\mathbf{K^T S_\epsilon}^{-1}\mathbf{K} \qquad \mathbf{S_m} = (\mathbf{K^T S_\epsilon}^{-1}\mathbf{K} + \mathbf{S_r})^{-1}\mathbf{K^T S_\epsilon}^{-1}\mathbf{K}(\mathbf{K^T S_\epsilon}^{-1}\mathbf{K} + \mathbf{S_r})^{-1} \tag{7}$$

The square root values of the diagonal elements of the retrieval noise covariance matrix $\mathbf{S_m}$ will be referred to as the theoretical precision of the retrieval. The vertical resolution of the retrieved profile is computed as the inverse of the diagonal elements of the averaging kernel matrix, multiplied by the altitude layer width. Examples of averaging kernels, vertical resolution and theoretical precision are plotted in Fig. 7. One can notice that below 35 km the actual vertical resolution of the retrieval scheme is about 2–3 km with a peak around 35 km where the transition between UV and Vis spectral ranges occurs. The theoretical precision of the retrieved ozone profiles doesn't show a strong dependence on the solar zenith angle. It lies in the range 1–5 % between 25 and 50 km and tends to increase in the upper stratosphere and in the Upper Troposphere - Lower Stratosphere (UTLS) region.

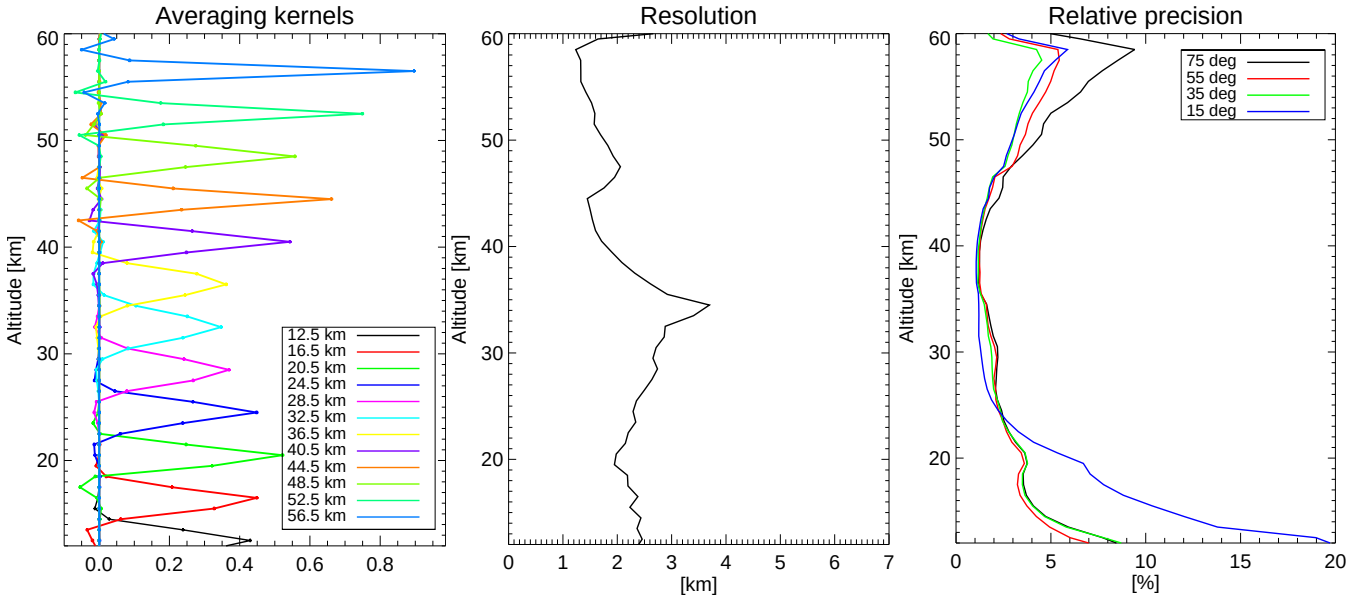

Figure 7. From left to right, examples of averaging kernels (plotted every 4 km for sake of clarity), vertical resolution and theoretical precision of the retrieval scheme. AKs and vertical resolution are plotted for a measurement at 30° N, whereas theoretical precision is shown for several observations in the same orbit but at different solar zenith angles (the black line lies behind the green one below 25 km).

4.2 Comparison with NASA OMPS-LP ozone product

To retrieve ozone profiles from OMPS-LP observations, the NASA team implemented the Environmental Data Record algorithm, based on the Optimal Estimation approach with a priori constraints. In this procedure, a series of secondary parameters such as surface albedo, cloud height and TH correction are derived before the main retrieval of ozone profiles (Rault and Loughman, 2013). Two spectral ranges are used for the latter task: UV wavelengths between 29.5 and 52.5 km and wavelengths in the Chappuis band between 12.5 and 37.5 km (the bottom height depends on the detected cloud top altitude). The normalization of the radiance is performed with respect to high altitude TH measurements: 55.5 km in UV and 40.5 km in Vis. The measurement vector is obtained using the doublet and triplet method respectively for the Hartley-Huggins and Chappuis bands; more details are given in Table 2. An additional TH correction is applied by NASA team on L1G data, as described in the Release Notes (DeLand et al., 2017). The quality flag related to the South Atlantic Anomaly is taken into consideration for the following comparison (Kahn and Kowitt, 2015).

In version 2.5 of NASA L2 data, independent profiles for the Vis and UV retrieval are provided. Fig. 8 shows a comparison between NASA-OMPS retrievals and our results (in the following called IUP-OMPS), considering the two retrieved profiles independently. Panel (a) presents an example of averaged profiles in terms of number density for the tropics. In panels (b) and (c), relative differences are shown for the tropical region, southern and northern mid-latitude bands. Throughout the paper,

Table 2. Wavelengths used in the NASA-OMPS ozone retrieval, according to DeLand et al. (2017)

Parameters	Values
Doublet λ_0	353 nm
Triplet λ_l	510 nm
Triplet λ_r	675 nm
Wavelength used in UV (nm)	302, 312, 322
Wavelength used in Vis (nm)	600

relative differences are computed as:

$$\text{Rel diff} = \frac{2 * (\text{IUP-OMPS - Reference data set})}{(\text{IUP-OMPS + Reference data set})} * 100 \quad (8)$$

Considering the Vis NASA retrieval in panel (b), the agreement is particularly good for the tropical region above 20 km, as it is also in panel (a). Looking at mid-latitudes, IUP-OMPS values are generally higher with respect to the NASA product, especially between 22 and 32 km. In the lower stratosphere we can notice larger differences between the two profiles in all latitude bands. Considering the UV NASA retrieval in panel (c), an agreement within ±5 % is found in almost all the cases, even if higher values are shown by IUP-OMPS around 45 km at mid-latitudes.

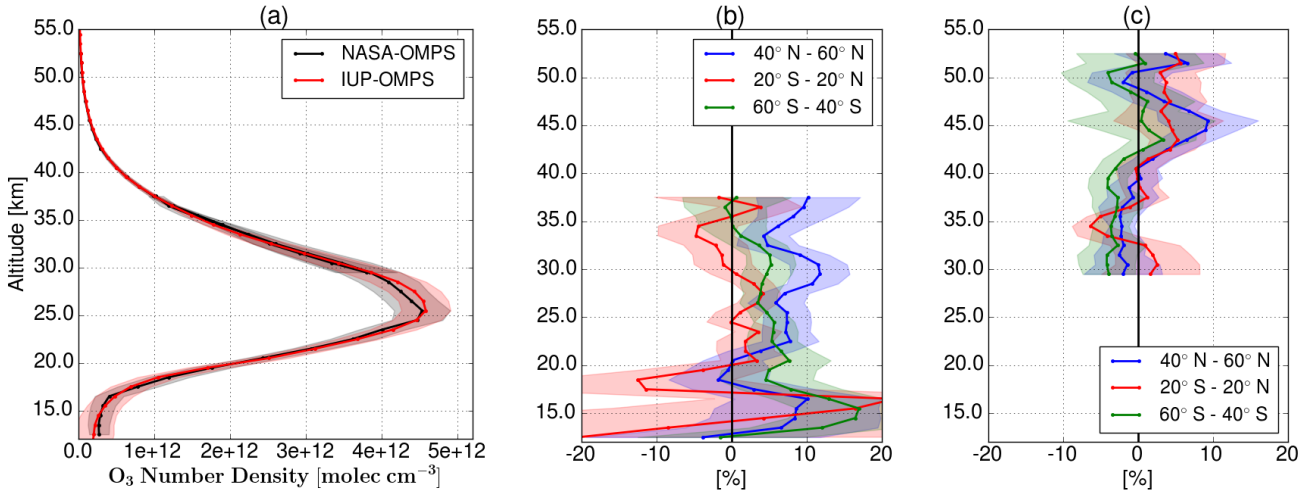

Figure 8. Panel (a): IUP-OMPS and NASA-OMPS retrieved number density profiles averaged in the tropical region. Panel (b) and (c): relative differences (Eq. 8) for the Vis and UV retrievals, respectively, are shown in three latitudinal bands (40° N–60° N, 20° S–20° N and 60° S–40° S), with corresponding standard deviations as shaded areas.

4.3 Comparison with MLS

The MLS instrument was launched on board the Aura satellite in July 2004 to observe the thermal emission from atmospheric trace gases in the millimeter/sub-millimeter spectral range. It scans the Earth limb 240 times per orbit, providing retrievals of daytime and nighttime profiles of several gases. For a detailed description of the MLS instrument refer to Waters et al. (2006). In this paper, the version 4.2 of MLS L2 data is used for the validation. Quality flags and recommendations reported in Livesey et al. (2017) are taken into consideration for the following analysis. Because of the large amount of available data, tight collocation criteria are applied to find collocated measurements. The geographic distance between the centers of the two instrument footprints is limited to be within 1° latitude and longitude and the time difference is required to be within 6 h. In addition, the difference in the potential vorticity at 20.5 km is required to be less than 5 PVU, in order to avoid collocation of measurements inside and outside the polar vortex. Information about potential vorticity is taken form the European Center Medium Weather Forecast (ECMWF) database (ERA interim). OMPS-LP states affected by the presence of PMCs and observations at altitudes flagged as cloudy are rejected. In case of multiple MLS collocations for the same OMPS-LP measurement, only the closest one is taken into consideration. To be consistent with NASA and sonde comparisons, MLS profiles are converted from VMR vs. pressure into number density vs. altitude (using MLS geopotential height), interpolated at the regular altitude grid of IUP-OMPS retrieved profiles and finally zonally averaged. Three latitudinal bands are selected for the comparison: 40° N–60° N, 20° S–20° N and 60° S–40° S. Fig. 9 shows the averaged profiles for the tropics and relative differences (Eq. 8) in the three latitudinal bands. Standard deviations are reported in the plots as shaded areas. The number of collocations per band is ∼ 5000.

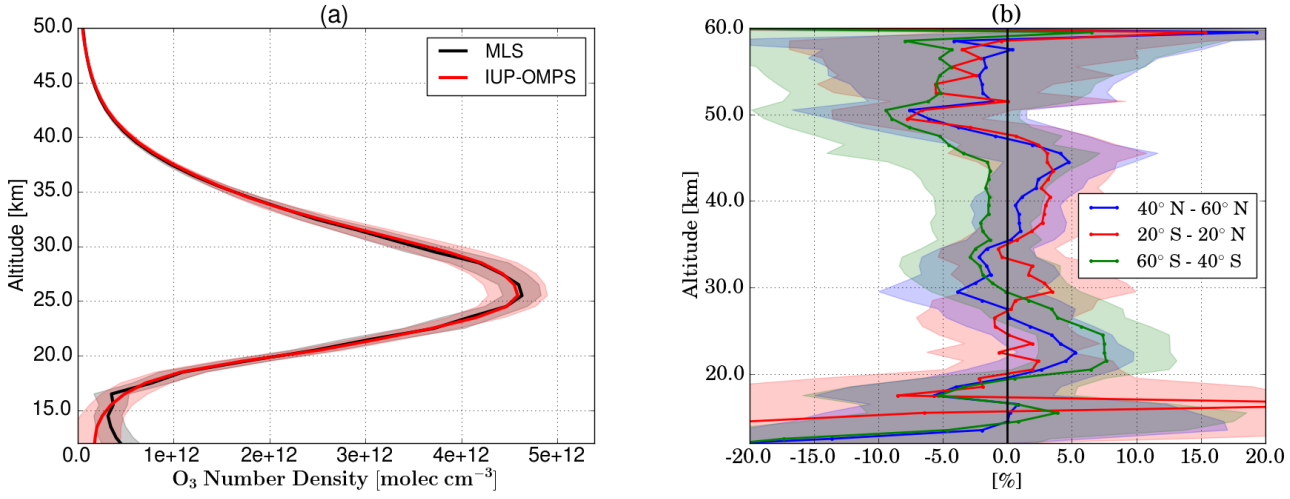

Figure 9. Panel (a): collocated IUP-OMPS retrieved profiles and MLS ozone product in the tropical region. Panel (b): relative difference profiles (Eq. 8) in three latitudinal bands (40° N–60° N, 20° S–20° N and 60° S–40° S), with standard deviations shown as shaded areas.

Fig. 10 shows the relative differences between IUP-OMPS and MLS zonal means binned in 2.5° wide latitude bins as a function of altitude. Three time periods are considered in the panels. In panel (a), showing all 6 months of data, we can see

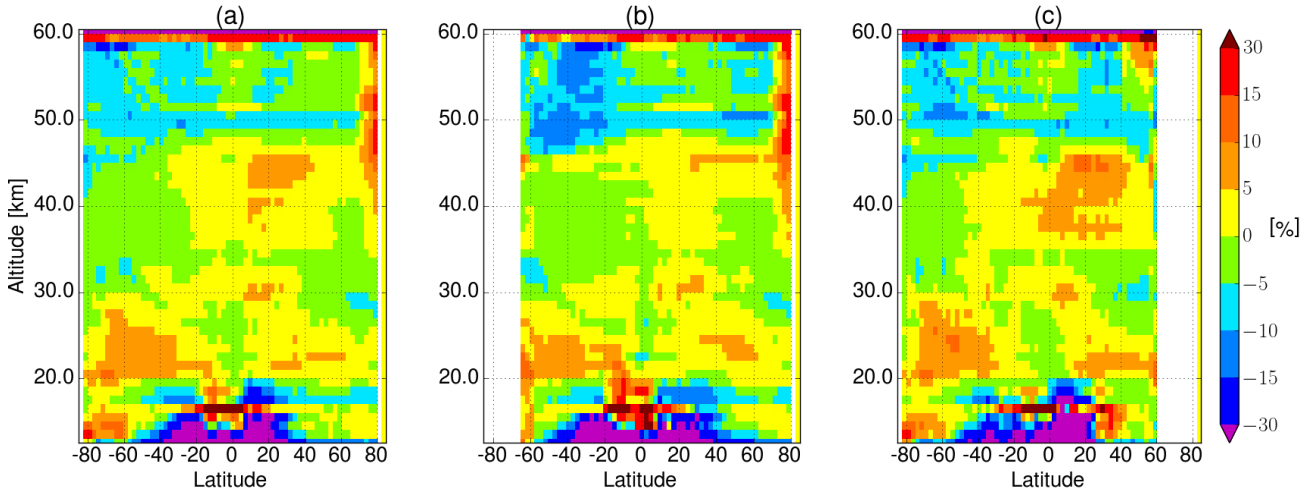

Figure 10. Relative differences (Eq. 8) averaged over 2.5° latitude bins, plotted as a function of altitude. Panel (a) 6 months, panel (b) July and August, panel (c) December and January

that between 20 and 50 km the differences are generally within ±10 %. Starting the discussion from the bottom of the plots, positive differences larger than 30 % are found in the tropical UTLS region. This large discrepancy can be related to multiple factors such as different vertical resolutions of the instruments, generally low sensitivity to ozone in the lowermost retrieval altitude range or issues with the cloud filtering. At mid-latitudes around 25 km a positive difference of 5–10 % is observed. This bias can be related to the water vapor treatment inside the retrieval scheme: the intensity of the ozone number density peak is found to be sensitive to the choice of the spectral points that are skipped in the Chappuis band, where H_2O has non-negligible absorption. Around 45 km, higher values are shown by IUP-OMPS at northern mid-latitudes, especially during winter months (panel c). This issue, already found in Fig. 8 panel (c), can be related to a problem in the junction between the spectral ranges in the Hartley and Huggins bands, that occurs indeed at 46 km. We also notice a significant discrepancy towards northern latitudes (> 70°) above 40 km; this disagreement can be partly related to the stray light affecting the TH normalization at 63 km. Looking at panel (b) we notice that the discrepancy increases: these are months when PMCs are expected. This is an indication of a sub-optimal screening of these clouds in IUP-OMPS data, while MLS observations are found not to be affected by the presence of PMCs (Bak et al., 2015). Above 50 km lower values than those from MLS are found in the southern hemisphere: this can be related to a pointing issue of the instrument as described in Sect. 2.2. Furthermore, a dip around 50 km can be noticed, which is most probably related to the TH normalization chosen for the Huggins band, and artificial oscillations appear evident at the two uppermost levels. An increase of the Tikhonov parameter is expected to attenuate the latter problem. To summarize, this comparison shows a general validity of IUP-OMPS retrieval between 18 and 58 km, even if during different seasons the relative bias with respect to MLS exceeds by 10 % in some limited atmospheric regions.

4.4 Comparison with ozonesondes

Ozonesonde data are obtained from WOUDC (World Ozone and Ultraviolet Radiation Data Center) and SHADOZ (Southern Hemisphere ADditional OZonesondes, Thompson et al., 2007) archives. We selected looser collocation criteria compared to MLS, because of the sparseness of ozonesonde measurements. Therefore, OMPS-LP measurements are required to be within 5° in latitude and 10° in longitude from the ozonesonde station and within ± 12 h time span around the sonde launch. For each sonde profile, all collocated OMPS-LP observations are averaged before the comparison. Ozonesonde profiles are smoothed to the vertical resolution of the OMPS-LP retrieval grid, by using the AKs as follow. First, we calculate the linear interpolation matrix $\mathbf{L}$ to map the low resolution OMPS profile onto the fine sonde grid. Then this matrix is inverted using the pseudo-inverse formulation (Rodgers, 2000), obtaining $\mathbf{L}^*$ as:

$$\mathbf{L}^* = (\mathbf{L}^T\mathbf{L})^{-1}\mathbf{L}^T \tag{9}$$

The ozonesonde high resolution profile $\boldsymbol{x_{fine}}$ is smoothed then as follows:

$$\boldsymbol{x_{coarse}} = \mathbf{A}\ \mathbf{L}^*\ \boldsymbol{x_{fine}} \tag{10}$$

The upper altitude of the smoothed profile is chosen at the OMPS-LP grid level whose corresponding AK altitude range is fully covered by the sonde profile. An approach alternative to the AK smoothing assumes a simple vertical average, considering 2.5 km (i.e $\pm$ 1.25 km) ranges around each grid point (value corresponding to an average vertical resolution of the retrieval scheme below 30 km, refer to Fig. 7). The altitude where a cloud is detected and all altitudes below are screened out. Latitude bins are selected as for the previous comparisons. Fig. 11 shows averaged collocated profiles in the tropical and northern mid-latitude bands with corresponding standard deviations. On the left side of these plots, the number of available collocations at each altitude is reported, which is about 120 and 160 for tropical and northern mid-latitude bands, respectively.

Fig. 12 shows the relative differences (Eq. 8) in the three latitudinal bands, in panel (a) using the averaging kernel smoothing approach and in panel (b) the vertical averaging. Differences between the two panels of this figure show that the smoothing procedure can be critical in the comparison between 15 and 20 km, where the gradient in the ozone profile is usually strong. The lack of stations at northern and southern high latitudes prevents a meaningful comparison over this short time span. As shown in Figs. 11 and 12, an excellent agreement is found at northern mid-latitudes, with relative differences within $\pm$ 5 % between 14 and 30 km. Focusing on the tropical region, a bias between the two data sets is clearly visible, with differences around 5–20 % between 18 and 32 km. This positive bias is unexpected considering the good agreement found when comparing to MLS data in the same region. In the UTLS region we also notice a peak of deviation; at these altitudes, ozone is hard to retrieve due to its decreasing concentration and the smoothing procedure may also introduce artifacts in the sonde profiles. Finally, at southern mid-latitudes, we notice a difference around 10 % between 20 and 30 km and a better agreement below. However, in this case, the validation is less significant because only two ozonesonde stations and about 25 comparisons are available within the considered time span.

With respect to the bias found in the tropical region, the processing of the OMPS-LP 2013 data set is also performed using the same retrieval settings. The analysis of these results and their validation against ozonesondes reveal a much smaller bias

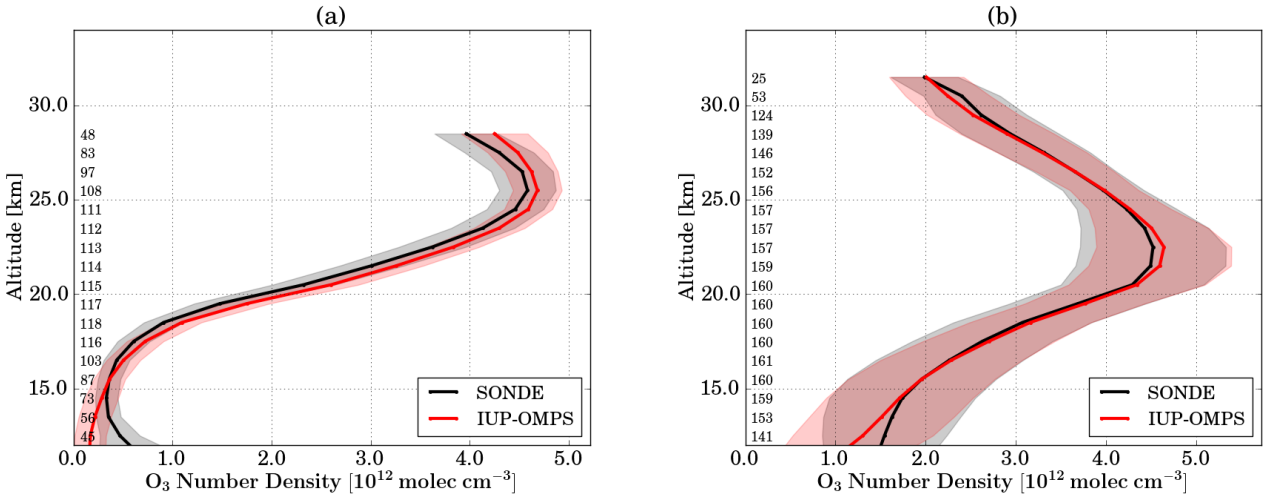

Figure 11. Comparison between collocated IUP-OMPS profiles and ozonesonde measurements in the latitudinal bands 20° S–20° N in panel (a) and 40° N–60° N in panel (b); standard deviations are shown as shaded areas.

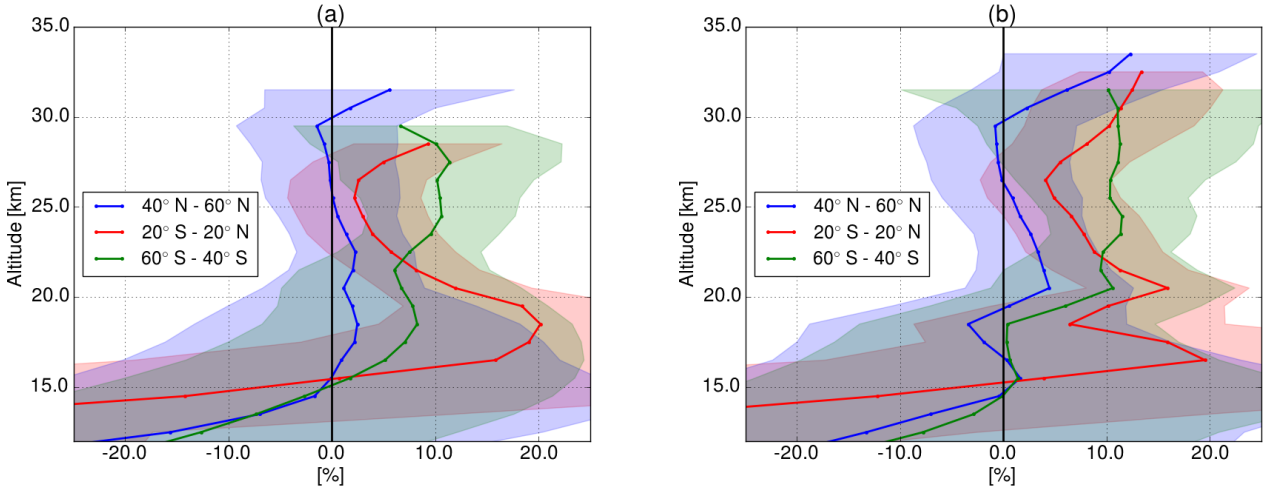

Figure 12. Relative differences between collocated IUP-OMPS profiles and ozonesonde measurements in three latitudinal bands (40° N–60° N, 20° S–20° N and 60° S–40° S), using in panel (a) averaging kernel smoothing and in panel (b) vertical averaging. Corresponding standard deviations are shown as shaded areas.

in the tropics. Relative differences between IUP-OMPS and sonde profiles in the same three latitudinal bands are shown in Fig. 13, following the averaging kernel smoothing approach. Since most of the sondes considered over the period Jul 2016–Jan 2017 come from the SHADOZ archive, we also take only measurements from the same archive for the 2013 validation: over the whole year, around 140 collocations are available from 10 stations. In Fig. 13, focusing the attention on the differences

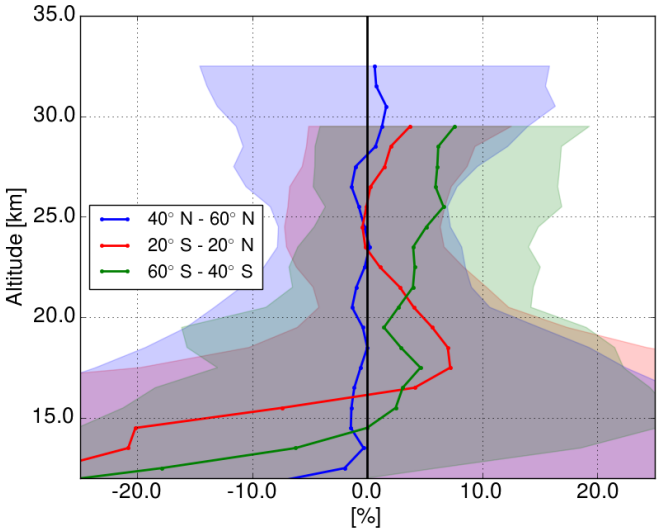

Figure 13. Relative differences between collocated IUP-OMPS profiles and ozonesonde measurements in three latitudinal bands (40° N–60° N, 20° S–20° N and 60° S–40° S) for the 2013 data set, with corresponding standard deviations as shaded areas.

in the tropical region, we can see that at least between 20 and 30 km the bias is within 5 %; larger discrepancies are still evident in the lower stratosphere. A comparison with MLS shows a very similar pattern to the one found for the 2016 data set. Further investigations of possible reasons for the observed behavior are ongoing. Concluding, we find a general consistency of IUP-OMPS retrieval results with ozonesonde measurements in all considered latitude bands, except for the 12–20 km altitude range in the tropics, where the agreement with SHADOZ ozonesondes is ambiguous.

5 Conclusions

The retrieval algorithm originally developed at the University of Bremen to obtain vertical distributions of ozone from SCIAMACHY limb measurements was tailored and applied to OMPS-LP observations. Seven months (Jul 2016–Jan 2017) of v2.5 L1G data were processed, analyzed and validated. Ozone profiles were retrieved between 12 and 60 km, considering only the central slit of the instrument and observations at a solar zenith angle less than 80°. A comparison with NASA v2.5 L2 official product was carried out, showing a general good agreement in the tropics, with discrepancies within ± 5 % between 20 and 52 km, and a bias of about 10 % at 30 and 45 km at northern mid-latitudes. We presented the results of the validation against MLS v4.2 ozone profiles and ozonesonde measurements from SHADOZ and WOUDC archives. A good agreement was found with the MLS ozone product: relative differences were generally within ± 5 % between 15 and 48 km. On the other hand, we observed a larger discrepancy between IUP-OMPS retrievals and MLS in the tropical UTLS region, related most probably to the decreasing sensitivity of limb retrievals from both instruments in this region. A discrepancy above 10 % in the upper strato-

sphere beyond 70° N is related to a sub-optimal PMC screening. In regard to the comparison with ozonesondes, at northern mid-latitudes differences within $\pm$ 5 % were found between 14 and 30 km. Focusing on the tropical region, a consistent positive bias with SHADOZ measurements was detected, unexpected after the good agreement observed with MLS data. However, the processing and validation of the 2013 data set, using the same retrieval settings, revealed a much better consistency. The reasons for this behavior are still under investigation. In light of the results presented here, an additional work for tuning of some retrieval settings is needed before processing the whole data set and attempting the merging with the SCIAMACHY time series. Since the same 1-D retrieval approach has been used for both data sets, we expect this to ease the merging. Unfortunately, only a couple of overlapping months between the two instruments are available, so that a third product must be used for the merging. After the good agreement found in the comparison of our retrievals with MLS, we are considering the use of the latter instrument as a transfer function to handle calibration issues in the merging procedure.

6 Data availability

Ancillary information and v2.5 L1G OMPS-LP data were downloaded from https://ozoneaq.gsfc.nasa.gov/data/omps/, where L2 data are also available.

For the validation sections, MLS L2 data were taken from https://disc.gsfc.nasa.gov/datasets. WOUDC data were retrieved on May 18, 2017, from http://woudc.org; a list of all contributors is available on the following website: doi:10.14287/10000001. SHADOZ were retrieved on April 6, 2017 from https://tropo.gsfc.nasa.gov/shadoz/Archive.html. Our results are available upon request at the University of Bremen.

Author contributions. CA adapted the retrieval algorithm to OMPS-LP observations, processed the data set, performed the validation of the results and wrote the manuscript. AR provided the retrieval algorithm exploited in this study, supervised and guided the retrieval process and reviewed the paper. EM provided retrieved aerosol extinction profiles. K-UE contributed with the algorithm for cloud filtering that was adapted to OMPS-LP observations. TvC contributed to the discussion of the regularization matrices for the retrieval scheme and the proper use of averaging kernels to smooth the ozonesonde profiles and reviewed the paper. JPB, who proposed the research and leads the project, analyzed the results and contributed to the writing of the manuscript and the scientific outcomes.

Competing interests. The authors declare that they have no conflict of interests. TvC is associated editor of AMT but is not involved in the reviewing of this particular paper.

Acknowledgements. This work was partially funded by ESA within the Ozone CCI project and was supported by the University and State of Bremen. We would like to acknowledge NASA OMPS SIPS team (in particular G. Jaross, N. Kramarova and P.K. Bhartia) for the support provided during the data analysis as well as for the concession of the new v2.5 of OMPS-LP L1G data before its official release.

References

Aschmann, J., Burrows, J. P., Gebhardt, C., Rozanov, A., Hommel, R., Weber, M., and Thompson, A. M.: On the hiatus in the acceleration of tropical upwelling since the beginning of the 21st century, Atmospheric Chemistry and Physics, 14, 12 803–12 814, doi:10.5194/acp-14-12803-2014, http://www.atmos-chem-phys.net/14/12803/2014/, 2014.

Bak, J., Liu, X., Kim, J. H., Deland, M. T., and Chance, K.: Simultaneous Retrievals of Polar Mesospheric Clouds (PMCs) with Ozone from OMI UV measurements, Atmospheric Chemistry and Physics Discussions, 15, 25 907–25 932, doi:10.5194/acpd-15-25907-2015, https://www.atmos-chem-phys-discuss.net/15/25907/2015/, 2015.

Bhartia, P., Jaross, G., Larsen, J., and Fleig, A.: Science Team Evaluation of the OMPS Limb Profiler, Tech. rep., 2013.

Bogumil, K., Orphal, J., Burrows, J. P., et al.: Temperature dependent absorption cross sections of O3, NO2, and other atmospheric trace gases measured with the SCIAMACHY spectrometer, in: Proceedings of the ERS-Envisat-Symposium, Goteborg, Sweden, 2000.

Burrows, J., Hölzle, E., Goede, A., Visser, H., and Fricke, W.: SCIAMACHY—Scanning imaging absorption spectrometer for atmospheric chartography, Acta Astronautica, 35, 445–451, 1995.

Davis, S. M., Rosenlof, K. H., Hassler, B., Hurst, D. F., Read, W. G., Vömel, H., Selkirk, H., Fujiwara, M., and Damadeo, R.: The Stratospheric Water and Ozone Satellite Homogenized (SWOOSH) database: A long-term database for climate studies, Earth System Science Data, 8, 461, 2016.

DeLand, M., Bhartia, P., Xu, P., Kramarova, N., and Zhu, T.: OMPS Limb Profiler Ozone Product O3: Version 2.5 Data Release Notes, 2017.

Eckert, E., Clarmann, T. v., Kiefer, M., Stiller, G., Lossow, S., Glatthor, N., Degenstein, D., Froidevaux, L., Godin-Beekmann, S., Leblanc, T., et al.: Drift-corrected trends and periodic variations in MIPAS IMK/IAA ozone measurements, Atmospheric Chemistry and Physics, 14, 2571–2589, 2014.

Eichmann, K.-U., Lelli, L., von Savigny, C., Sembhi, H., and Burrows, J. P.: Global cloud top height retrieval using SCIAMACHY limb spectra: model studies and first results, Atmospheric Measurement Techniques, 9, 793–815, doi:10.5194/amt-9-793-2016, https://www.atmos-meas-tech.net/9/793/2016/, 2016.

Farman, J. C., Gardiner, B. G., and Shanklin, J. D.: Large losses of total ozone in Antarctica reveal seasonal ClOx/NOx interaction, Nature, 315, 207–210, 1985.

Flynn, L., Long, C., Wu, X., Evans, R., Beck, C., Petropavlovskikh, I., McConville, G., Yu, W., Zhang, Z., Niu, J., et al.: Performance of the ozone mapping and profiler suite (OMPS) products, Journal of Geophysical Research: Atmospheres, 119, 6181–6195, 2014.

Froidevaux, L., Anderson, J., Wang, H.-J., Fuller, R. A., Schwartz, M. J., Santee, M. L., Livesey, N. J., Pumphrey, H. C., Bernath, P. F., Russell III, J. M., and McCormick, M. P.: Global OZone Chemistry And Related trace gas Data records for the Stratosphere (GOZCARDS): methodology and sample results with a focus on HCl, H_2O, and O_3, Atmospheric Chemistry and Physics, 15, 10 471–10 507, doi:10.5194/acp-15-10471-2015, https://www.atmos-chem-phys.net/15/10471/2015/, 2015.

Gebhardt, C., Rozanov, A., Hommel, R., Weber, M., Bovensmann, H., Burrows, J., Degenstein, D., Froidevaux, L., and Thompson, A.: Stratospheric ozone trends and variability as seen by SCIAMACHY from 2002 to 2012, Atmospheric Chemistry and Physics, 14, 831–846, 2014.

Gottwald, M. and Bovensmann, H.: SCIAMACHY-Exploring the changing Earth's Atmosphere, Springer Science & Business Media, 2011.

Hassler, B., Petropavlovskikh, I., Staehelin, J., August, T., Bhartia, P., Clerbaux, C., Degenstein, D., Mazière, M. D., Dinelli, B., Dudhia, A., et al.: Past Changes in the Vertical Distribution of Ozone Part 1: Measurement Techniques, Uncertainties and Availability, 2014.

Hess, M., Koepke, P., and Schult, I.: Optical properties of aerosols and clouds: The software package OPAC, Bulletin of the American meteorological society, 79, 831–844, 1998.

Jaross, G., Bhartia, P. K., Chen, G., Kowitt, M., Haken, M., Chen, Z., Xu, P., Warner, J., and Kelly, T.: OMPS Limb Profiler instrument performance assessment, Journal of Geophysical Research: Atmospheres, 119, 4399–4412, 2014.

Jia, J., Rozanov, A., Ladstätter-Weißenmayer, A., and Burrows, J.: Global validation of SCIAMACHY limb ozone data (versions 2.9 and 3.0, IUP Bremen) using ozonesonde measurements, Atmospheric Measurement Techniques, 8, 3369–3383, 2015.

Kahn, D. and Kowitt, M.: Limb Gridded Radiance User Guide, LP-L1G-EV-1.0, version 2.0, Tech. rep., 2015.

Kyrölä, E., Laine, M., Sofieva, V., Tamminen, J., Päivärinta, S.-M., Tukiainen, S., Zawodny, J., and Thomason, L.: Combined SAGE II–GOMOS ozone profile data set for 1984–2011 and trend analysis of the vertical distribution of ozone, Atmospheric Chemistry and Physics, 13, 10 645–10 658, 2013.

Livesey, N., Read, W., Wagner, P., Froidevaux, L., Lambert, A., Manney, G. L., Millan Valle, L. F., Pumphrey, H. C., Santee, M. L., Schwartz, M. J., Wang, S., Fuller, R. A., Jarnot, R. F., Knosp, B. W., and Martinez, E.: Version 4.2x Level 2 data quality and description document, 2017.

Llewellyn, E., Degenstein, D., McDade, I., Gattinger, R., King, R., Buckingham, R., Richardson, E., Murtagh, D., Evans, W., Solheim, B., et al.: Osiris—An Application of Tomography for Absorbed Emissions in Remote Sensing, in: Applications of Photonic Technology 2, pp. 627–632, Springer, 1997.

Molina, M. J. and Rowland, F. S.: Stratospheric sink for chlorofluoromethanes: chlorine atom-catalysed destruction of ozone, Nature, 249, 810–812, 1974.

Moy, L., Bhartia, P. K., Jaross, G., Loughman, R., Kramarova, N., Chen, Z., Taha, G., Chen, G., and Xu, P.: Altitude registration of limb-scattered radiation, Atmospheric Measurement Techniques, 10, 167–178, 2017.

Nedoluha, G., Siskind, D., Lambert, A., and Boone, C.: The decrease in mid-stratospheric tropical ozone since 1991, Atmospheric Chemistry and Physics, 15, 4215–4224, 2015.

Rault, D. F. and Loughman, R. P.: The OMPS Limb Profiler environmental data record algorithm theoretical basis document and expected performance, IEEE Transactions on Geoscience and Remote Sensing, 51, 2505–2527, 2013.

Rieger, L., Malinina, E., Rozanov, A., Burrows, J. P., Bourassa, A., and Degenstein, D.: Error Estimation for Limb Scatter Aerosol Extinction Retrievals Using OSIRIS and SCIAMACHY, submitted to Atmos. Meas. Tech. on 8 Dec, 2017, 2017.

Rodgers, C. D.: Inverse methods for atmospheric sounding: theory and practice, vol. 2, World scientific, 2000.

Rozanov, A., Weigel, K., Bovensmann, H., Dhomse, S., Eichmann, K.-U., Kivi, R., Rozanov, V., Vömel, H., Weber, M., and Burrows, J.: Retrieval of water vapor vertical distributions in the upper troposphere and the lower stratosphere from SCIAMACHY limb measurements, Atmospheric Measurement Techniques, 4, 933–954, 2011.

Rozanov, A. V., Rozanov, V. V., and Burrows, J. P.: Combined differential-integral approach for the radiation field computation in a spherical shell atmosphere: Nonlimb geometry, Journal of Geophysical Research: Atmospheres, 105, 22 937–22 942, 2000.

Rozanov, V., Rozanov, A., Kokhanovsky, A., and Burrows, J.: Radiative transfer through terrestrial atmosphere and ocean: software package SCIATRAN, Journal of Quantitative Spectroscopy and Radiative Transfer, 133, 13–71, 2014.

Serdyuchenko, A., Gorshelev, V., Weber, M., Chehade, W., and Burrows, J. P.: High spectral resolution ozone absorption cross-sections – Part 2: Temperature dependence , Atmospheric Measurement Techniques, 7, 625–636, doi:10.5194/amt-7-625-2014, https://www.atmos-meas-tech.net/7/625/2014/, 2014.

Sofieva, V. F., Kyrölä, E., Laine, M., Tamminen, J., Degenstein, D., Bourassa, A., Roth, C., Zawada, D., Weber, M., Rozanov, A., Rahpoe, N., Stiller, G., Laeng, A., von Clarmann, T., Walker, K. A., Sheese, P., Hubert, D., van Roozendael, M., Zehner, C., Damadeo, R., Zawodny, J., Kramarova, N., and Bhartia, P. K.: Merged SAGE II, Ozone_cci and OMPS ozone profiles dataset and evaluation of ozone trends in the stratosphere, Atmospheric Chemistry and Physics Discussions, 2017, 1–28, doi:10.5194/acp-2017-598, https://www.atmos-chem-phys-discuss.net/acp-2017-598/, 2017.

Solomon, S., Ivy, D. J., Kinnison, D., Mills, M. J., Neely, R. R., and Schmidt, A.: Emergence of healing in the Antarctic ozone layer, Science, 353, 269–274, 2016.

Steinbrecht, W., Froidevaux, L., Fuller, R., Wang, R., Anderson, J., Roth, C., Bourassa, A., Degenstein, D., Damadeo, R., Zawodny, J., et al.: An update on ozone profile trends for the period 2000 to 2016 [Discussions paper], 2017.

Stiller, G. P., Fierli, F., Ploeger, F., Cagnazzo, C., Funke, B., Haenel, F. J., Reddmann, T., Riese, M., and von Clarmann, T.: Shift of subtropical transport barriers explains observed hemispheric asymmetry of decadal trends of age of air, Atmospheric Chemistry and Physics Discussions, 2017, 1–16, doi:10.5194/acp-2016-1162, https://www.atmos-chem-phys-discuss.net/acp-2016-1162/, 2017.

Thompson, A. M., Witte, J. C., Smit, H. G., Oltmans, S. J., Johnson, B. J., Kirchhoff, V. W., and Schmidlin, F. J.: Southern Hemisphere Additional Ozonesondes (SHADOZ) 1998–2004 tropical ozone climatology: 3. Instrumentation, station-to-station variability, and evaluation with simulated flight profiles, Journal of Geophysical Research: Atmospheres, 112, 2007.

Tikhonov, A. N.: Solution of incorrectly formulated problems and the regularization method, Soviet Math. Dokl., 4, 1035–1038, 1963.

Waters, J. W., Froidevaux, L., Harwood, R. S., Jarnot, R. F., Pickett, H. M., Read, W. G., Siegel, P. H., Cofield, R. E., Filipiak, M. J., Flower, D. A., et al.: The earth observing system microwave limb sounder (EOS MLS) on the Aura satellite, IEEE Transactions on Geoscience and Remote Sensing, 44, 1075–1092, 2006.

Zawada, D. J., Rieger, L. A., Bourassa, A. E., and Degenstein, D. A.: Tomographic retrievals of ozone with the OMPS Limb Profiler: algorithm description and preliminary results, Atmospheric Measurement Techniques Discussions, 2017, 1–26, doi:10.5194/amt-2017-236, https://www.atmos-meas-tech-discuss.net/amt-2017-236/, 2017.